Tissue deformation spatially modulates VEGF signaling and angiogenesis

Nicolas C. Rivron[a,1], Erik J. Vrij[a], Jeroen Rouwkema[b], Severine Le Gac[c], Albert van den Berg[c], Roman K. Truckenmüller[a,c], and Clemens A. van Blitterswijk[a]

[a]Department of Tissue Regeneration, MIRA Institute for Biomedical Technology and Technical Medicine, University of Twente, 7500 AE, Enschede, The Netherlands; [b]Department of Biomechanical Engineering, MIRA Institute for Biomedical Technology and Technical Medicine, University of Twente, 7500 AE, Enschede, The Netherlands; and [c]BIOS, Lab on a Chip group, MESA+ Institute for Nanotechnology, University of Twente, 7500 AE, Enschede, The Netherlands

Edited by Robert Langer, MIT, Cambridge, MA, and approved February 17, 2012 (received for review February 1, 2012)

Physical forces play a major role in the organization of developing tissues. During vascular development, physical forces originating from a fluid phase or from cells pulling on their environment can alter cellular signaling and the behavior of cells. Here, we observe how tissue deformation spatially modulates angiogenic signals and angiogenesis. Using soft lithographic templates, we assemble three-dimensional, geometric tissues. The tissues contract autonomously, change shape stereotypically and form patterns of vascular structures in regions of high deformations. We show that this emergence correlates with the formation of a long-range gradient of Vascular Endothelial Growth Factor (VEGF) in interstitial cells, the local overexpression of the corresponding receptor VEGF receptor 2 (VEGFR-2) and local differences in endothelial cells proliferation. We suggest that tissue contractility and deformation can induce the formation of gradients of angiogenic microenvironments which could contribute to the long-range patterning of the vascular system.

vascular patterning | blood vessels | morphogenesis | mechanical forces

Tissue deformation influences the development of the vasculature in the embryo (1) and in the contracting wound (2). Current models suggest that physical forces originating from the blood (3), from cells pulling on neighboring cells (4), and on the Extra Cellular Matrix (ECM) (5) distort cellular membrane receptors and cytoskeletal elements, modulate biochemical signaling pathways and the behavior of endothelial and smooth muscle cells (6). However it is not known whether physical forces can spatially modulates angiogenic signals and contribute to vascular patterning.

Angiogenic molecules orchestrate cellular behaviors (growth, apoptosis, mobility) whose local differentials underlie morphogenesis and the formation of vascular patterns. The Vascular Endothelial Growth Factor (VEGF) is a highly vascular-specific signaling molecule. The principal component of the VEGF molecules is VEGF-A, it binds the Receptor Tyrosine Kinase VEGF Receptor 2 (VEGFR-2). VEGFR-2 activates multiple downstream signaling molecules including Mitogen-Activated Protein Kinases (MAPKs), Phosphoinositide 3-Kinases, PKB (Protein Kinase B) or small GTPases (7). As a result, endothelial cells (EC) proliferate, migrate, degrade the ECM, and modulate endothelium permeability (7). The tight spatial regulation of the VEGF-A/VEGFR-2 system is thus essential to control vascular development. Interestingly, the growth and apoptosis of EC (8, 9) and the expression of VEGFR-2 (3, 10) are modulated by physical forces. This regulation might occur via the Rho inhibitor p190RhoGAP and the balance between antagonist transcriptions factors TFII-I (also known as GTF2I) and GATA-2 (5).

Vascular patterning is governed by oxygen deficiency (hypoxia) which controls the local production of VEGF via Hypoxia-Inducible Factor [HIF1α, (11)]. A gradient of VEGF overlays a gradient of hypoxia which orientates, attracts, and induces proliferation of new blood vessels (12). Upon irrigation of the tissue, hypoxia decreases and so does the production of VEGF. This patterning mechanism does not imply a role for the physical deformation of tissues.

Microfabricated platforms are powerful tools to recapitulate and systematically manipulate simplified cases of tissue morphogenesis with an intermediate complexity between 2D cell culture and model organisms (13). In this manuscript, we show a simple, cost-effective, widely applicable platform to assemble 3D, free-standing tissues. We manipulate tissue deformation and observe its impact on the formation of gradients of angiogenic microenvironments and angiogenesis.

Results

Self-Remodeling Microfabricated Tissues. We mimicked the early events of angiogenesis using a coculture of two cell types: human Umbilical Vein Endothelial Cells (hUVEC) as a well characterized EC type (14) and human Mesenchymal Stem Cells (hMSC) which can generate forces (15), produce VEGF-A (16) thus mimicking some aspects of interstitial stromal cells. Our microarray data, along with others (17), show that hMSC do not significantly express VEGFR-2. Indeed, in this coculture, immunofluorescence of VEGFR-2 was restricted to hUVEC (Fig. S1). We previously showed that this coculture supports the formation of a 3D network of PECAM-1$^+$ vascular structures (VS) (18).

We used conventional soft lithography and micromolding to form nonadherent agarose templates (Fig. 1*A*). On these templates, we assembled tissues by sequentially aggregating cells into microscale clusters and millimeter-scale tissues (Fig. 1*A*). Resulting tissues are free-standing and biomaterial-free and can easily be manipulated (Fig. 1*B*). Tissues have an initial projection area of 1 mm^2 and a height of 250 μm. Over five days of culture, tissues contracted autonomously, deformed stereotypically, and finally stabilized their shapes (Fig. 1*C*, Fig. S2). Disc-shaped tissues deformed isotropically (Fig. 1*C*, first row) whereas square-shaped tissues deformed anisotropically. Corners displaced and deformed more as compared to sides (Fig. 1*C*, second row, Fig. S2, $p = 0.0015$, $n = 10$). To compensate, we designed star-shaped tissues which progressively deformed into a square (Fig. 1*C*, third row). This anisotropic deformation suggested a heterogeneous distribution of internal forces. It was previously modeled that boundaries and sharp geometries generate greater forces as compared to regions away from these boundaries (9, 19, 20). Based on macroscopic behavior and cellular density, we

Author contributions: N.C.R., J.R., R.K.T., and C.A.v.B. designed research; N.C.R. and E.J.V. performed research; S.L.G. and A.v.d.B. contributed new reagents/analytic tools; N.C.R. and J.R. analyzed data; and N.C.R. wrote the paper.

The authors declare no conflict of interest.

This article is a PNAS Direct Submission.

Freely available online through the PNAS open access option.

[1]To whom correspondence should be addressed. E-mail: nicolasrivron@gmail.com.

This article contains supporting information online at www.pnas.org/lookup/suppl/doi:10.1073/pnas.1201626109/-/DCSupplemental.

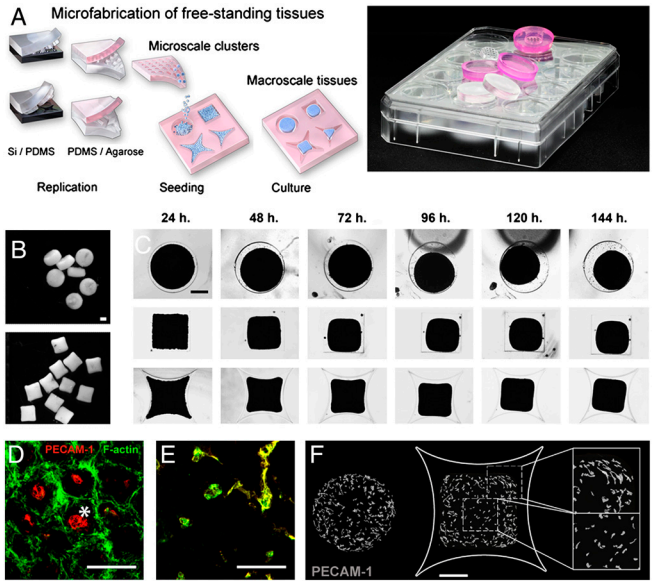

Fig. 1. Microfabricated tissues deform autonomously and form vascular structures in regions of high deformations. (*A*) Arrays of 3D millimeter-scale tissues are assembled by sequential aggregation of cells and microscale cell clusters in nonadherent micromolded wells. Arrays are replicated from PDMS stamps (transparent arrays) into agarose (pink arrays) and inserted in standard tissue culture plates. (*B*) Resulting tissues are 3D, millimeter-scale, free-standing and biomaterial-free (scale bar, 500 μm). (*C*) Microfabricated tissues contract, deform isotropically (top row) or anisotropically (second/third rows), and finally stabilize their shape (scale bar, 500 μm). (*D–E*) PECAM-1 is depicted in red and F-actin in green. Microscale cell clusters of hUVEC and hMSC first spontaneously form a PECAM-1$^+$ core [*D*, asterisk, (scale bar, 100 μm)] and a PECAM-1$^-$ external layer. Microscale cell clusters generate an F-actin intense interface upon fusion with neighbors (24 h). (*E*) After 24 h, PECAM-1$^+$ cells are F-actin$^+$ and start sprouting [*E*, (scale bar, 100 μm)]. (*F*) Upon tissue deformation, PECAM-1 immunostaining reveals a preferential formation of VS in regions of high deformations [tissue periphery and corners, (scale bar, 500 μm)].

estimated the local strain to be twofold higher in tissue corners as compared to tissue centers (Fig. S3).

Endothelial Cell Sprouting and the Formation of Patterns of Vascular Structures. In microscale clusters (first step, Fig. 1*A*, top row), hUVEC and hMSC separated into a core of PECAM-1$^+$ cells (asterisk, Fig. 1*D*) and an external layer of PECAM-1$^-$ cells. Sorting probably occurred according to differences in cellular affinity (strength of adhesion molecules) and cortical tension which determines cell association (21). When pooled (second step, Fig. 1*A*, bottom row), microscale clusters fused with neighbors via the transient and peripheral expression of filamentous actin (F-actin, Fig. 1*D*, 24 h, Fig. S4). After 24 h, PECAM-1$^+$ cells became F-actin intense, sprouted into VS (Fig. 1*E*) which branched and formed cord-like structures including few lumens. VS did not undergo full tubulogenesis but rather form small, interspersed lumens as described previously (18). This model is relevant to the early stage of vascular morphogenesis (13, 18, 20, 22). Angiogenic factors were produced locally by cells cultured in serum-free medium without any growth factors. Tissues contracted and deformed autonomously (no external forces applied). This model allows to couple endogenous tissue contractility and deformation to the formation of VS.

Upon tissues contraction and deformation (day 5), VS had formed preferentially in peripheral regions (Fig. 1*F*). The preferential formation of VS was consistently observed in disc-, star-, and triangle-shaped tissues (Fig. 1*F*, Fig. S5). In star- and triangle-shaped tissues, VS formed at higher density in corners as compared to sides ($p = 0.0026$ and $p = 0.002$ respectively, Fig. S5). We concluded that VS formed preferentially in regions of higher deformation.

Actin-Myosin Regulates Tissue Deformation. We impaired tissue contractility by blocking force-generating elements in cells. Non muscle Myosins II A, B, and C (NMM II) and F-actin are likely to be main generators of forces in hMSC (15). Blebistatin blocks the activation of NMM II ATPase and impairs its interaction with F-actin (23). Y27632 suppresses p160ROCK (Rho associated coiled-coil containing protein kinase) thus inhibiting the phosphorylation of Myosin Light Chain and the formation of F-actin stress fibers (23). Upon culture with Blebistatin or Y27632 alone, tissues contracted and deformed similarly to controls. However, upon exposure to the combination of the two inhibitors, tissues rapidly relaxed from 78% to 84% of their initial area (Fig. 2*A* and *B*, see black arrow, $p = 0.0002$, $n = 10$). This relaxation demonstrated an internal tensional state generated by the actin-myosin complex. Upon inhibition of actin and myosin, tissue contraction was later impaired (Fig. 2*A* and *B*, 144 h, 70% of the initial projected area vs. 58%, $p = 6.10^{-7}$, $n = 10$). Tissue contraction was impaired but not stopped which implies a possible contribution of other cytoskeletal components or mechanisms. Based on cellular density and macroscopic behavior, we estimated the overall strain to be twofold lower when contraction was impaired (Fig. S3).

Tissue Contraction Regulates the Gene Expression of VEGF-A and VEGFR-2. To investigate the molecular changes underlying tissue contraction, we compared the expression of angiogenic genes in tissues undergoing normal and impaired contraction. Expression levels of ECM genes (collagen type I, laminin α1, laminin β5) and matrix-degrading metalloproteinase genes (MMP9, MMP13) remained unchanged. However, expression levels of VEGF-A and VEGFR-2 were higher in contracting tissues as compared to tissue with impaired contraction (day 3, Fig. 2*C*). We tested the contribution of VEGF to the formation of the VS by adding a scavenging antibody to the culture medium. Addition of the VEGF antibody dramatically reduced the formation of VS, demonstrating thus a critical dependence of VS upon VEGF (Fig. 2*D*). In a control assay, we showed, in cell pellets, that the VEGF antibody prevented the formation of VS by decreasing cellular proliferation (Fig. S6). We concluded that VEGF was

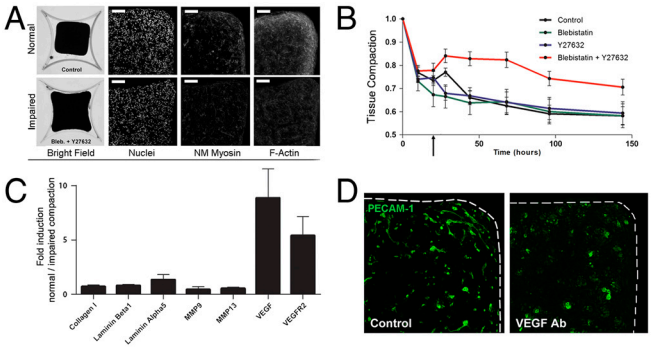

Fig. 2. Tissue deformation is actin-myosin dependent and regulates VEGF-A and VEGFR-2 expression. (*A*, *B*) The combined inhibition of non muscle Myosin II (Blebistatin) and Rho associated protein kinase p160ROCK (Y27632) at 24 h (see black arrow in *B*) induces a relaxation of the internal tissue tension (28 h) and impairs tissue deformation (150 h). (*A*, top row) Tissue deformation results in local compaction (nuclear, DAPI staining) and a concentration of force-generating elements [nm Myosin II and F-actin immunofluorescence, (scale bar, 100 μm)] in regions of high deformations. (*A*, bottom row) This effect is impaired when deformation is impaired. (*C*) Upon impairment of tissue deformation, expression levels of VEGF-A and VEGFR-2 are lower. ECM related genes remain similar. Standard deviations, $n = 3$. (*D*) The formation of VS is strongly impaired when a VEGF scavenging antibody is added to the culture medium (PECAM-1 immunofluorescence).

necessary for the formation of VS and that tissue contraction did not directly induce the formation of VS.

Local Tissue Compaction Partially Contributes to the Formation of Vascular Patterns. We then asked if the anisotropic deformation of tissues resulted in local changes in cellular density. Upon tissue contraction and deformation, cellular density gradually increased from the tissue center to the periphery (Fig. 2*B*, 3*A*). This gradient was impaired when contraction was impaired (Fig. 2*B*, 3*A*) and correlated with an increase of NMM II and F-actin (Fig. 2*B*).

We then assessed the contribution of local tissue compaction on the local formation of VS. Cellular density was homogeneous in the tissue center but gradually increased in the peripheral regions (Fig. 3 *A* and *B*). In parallel, the density of VS increased by 4.8-fold and the density of VS/nucleus increased by 2.5-fold (Fig. 3 *A* and *B*). When tissue contractility was impaired, the gradient of cellular density was impaired and VS grew homogeneously throughout the tissues (Fig. 3 *A* and *B*). Higher local cellular density directly contributed to 48% of the increased density of VS (Fig. 3*D*). This measurement assessed that local tissue compaction induced more than a direct concentration of VS and suggested a more complex role for endogenous contractile forces. Indeed, upon impairment of tissue contraction, the contribution of cellular density increased to 73% (Fig. 3*D*).

Tissue Contraction Induces Changes in the Phenotype of Vascular Structures. The phenotypes of VS changed across the tissue. In regions of high deformations, VS were thin, shaped and elongated perpendicular to the tissue displacement (Fig. 3*C*, left, white arrow shows the corner-to-center direction). This orientation of VS correlates with previous reports describing an elongation of EC perpendicular to externally applied mechanical stress (24). When endogenous contractility was impaired, VS grew homogeneously, were wider, tortuous, and randomly oriented (Fig. 3*C* right).

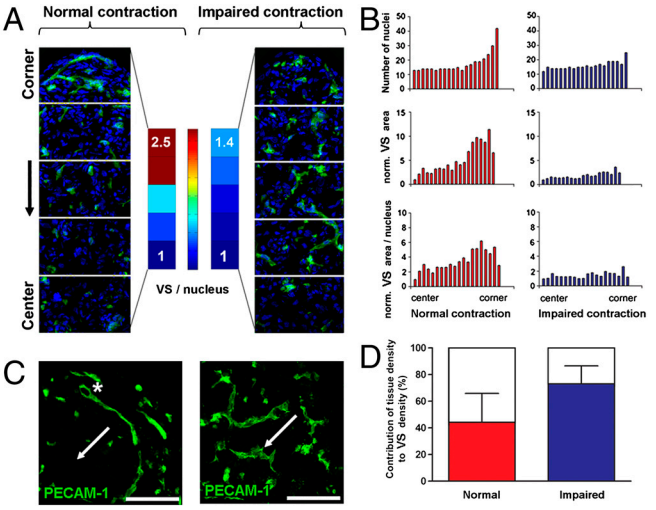

Fig. 3. Local tissue compaction partly contributes to the local formation of Vascular Structures. (*A*, *B*) VS form at a higher density in regions of high deformation (*A*, *B*, left, from the center to periphery: 2.5-fold increase in VS/nucleus). When tissue contraction and deformation are impaired, VS grow homogeneously throughout the tissue (*A*, *B* right). (*B*, *C*) Tissue deformation induces local tissue compaction (*B*, number of nuclei, top row) and the formation of thin VS including some lumens (asterisk, *C* left). VS preferentially elongate perpendicular to tissue displacement (*A*, *C*, arrows show the direction of displacement). This phenotype and directionality are impaired when contraction and deformation are impaired [*A*, *C*, right, (scale bars, are 100 μm)]. (*D*) Local tissue compaction partially contributes to the local formation of VS. The local increase in cellular density accounts for 48% of the local increase of VS (*D*, left, normal contraction). This contribution increases to 73% when contraction is impaired (*D*, right).

Vascular morphogenesis can be driven by local tissue hypoxia which regulates the production of multiple angiogenic factors (11). Tissues were designed with dimensions alleviating the formation of a hypoxic environment. However, we tested the possible formation of local hypoxic environments by looking at the distribution of HIF1α which translocates to the nuclei of hypoxic cells to activate angiogenic genes (11). Here, HIF1α was cytoplasmic and homogeneously expressed across the tissues. The cytoplasmic expression of HIF1a suggests that hypoxic levels are low and homogeneous across the tissues (Fig. S7).

Tissue Contractility Locally Regulates the Expression of VEGFR-2. EC are mechanosensitive cells (10, 20) which can transcriptionally regulate the expression of the VEGFR-2 receptor based on the mechanical properties of the microenvironment (5, 10). VEGFR-2 mediates the major growth and permeability roles of VEGF-A (5). Based on the differences in VEGFR-2 gene expression level (Fig. 2*C*), we tested the possibility that EC respond to tissue deformation by spatially modulating the expression of VEGFR-2. VEGFR-2 expression was restricted to PECAM-1$^+$ cells (Fig. S1), a cell-cell adhesion molecule which is thought to convey mechanical forces but whose expression is not regulated by mechanical forces (3). Upon tissue contraction, PECAM-1$^+$ cells in regions of high deformation expressed a higher level of VEGFR-2 per PECAM-1$^+$ area (8.5-fold increase) than cells in the central region ($p = 0.026$, $n = 15$, Fig. 4 *A* and *C*). When contraction was impaired, the expression of VEGFR-2/PECAM-1$^+$ area decreased and became homogenous across the tissue (Fig. 4 *A* and *C*). This local increase in VEGFR-2 expression correlated with the formation of clusters of high fluorescent intensity at the cellular membrane (Fig. S1). This observation is consistent with previous reports describing the formation of VEGFR-2 complexes in response to mechanical shear stress (10). The region of VEGFR-2 overexpression was very localized (last 20% of the center to periphery distance). We concluded, based on the mRNA expression level (Fig. 2*C*) and on the differential in immunofluorescent intensity, that endogenous tissue contractility induced a quantitative and spatial regulation of the VEGFR-2 receptor.

Tissue Contractility Regulates the Formation of a Gradient of VEGF. Based on the differences in VEGF-A gene expression level (Fig. 2*C*) and because hMSC are mechanosensitive cells (15), we tested the possibility that tissue contractility spatially regulated the expression of VEGF-A proteins. We cut the tissue corners and observe that the expression of VEGF-A mRNA was 1.5-fold higher in corners as compared to centers ($n = 3$, $p = 0.07$, Fig. S8*A*). Immunofluorescent staining (all VEGF isoforms) revealed the formation of a gradient of VEGF: fluorescent intensity in tissue corners was twofold higher than in tissue centers (Fig. 4 *B*, *D* and *E*). When contraction was impaired, the gradient of VEGF fluorescent intensity was impaired (Fig. 4*E*) and the total fluorescent intensity expressed in the tissue decreased by twofold ($p = 0.032$, $n = 3$, Fig. 4*F*). Upon normalization to the number of nuclei, cells in the regions of high deformation had higher fluorescent intensity as compared to cells located in the center ($p = 0.034$, $n = 15$, Fig. 4*F*). We assessed the validity of the measurement of fluorescent intensity using a 2D assay: Deferoxamine [DFO, a HIF-1a inducer (25)] induces a twofold increase in VEGF imunofluorescent staining intensity. This increase correlated with a fivefold increase in the intracellular production of VEGF (ELISA assay for isoforms 165 and 121 on cell lysate, Fig. S9). We further assessed the role of cell-generated forces on the production of VEGF proteins in cell pellets (0.5 million cells, 92% hMSC, and 8% hUVEC). Pellets whose contraction was impaired produce 1.6-fold less VEGF proteins than pellets undergoing normal contraction (Fig. 4*G*, ELISA assay on culture medium, $n = 3$, $p < 0.001$). These observations suggest

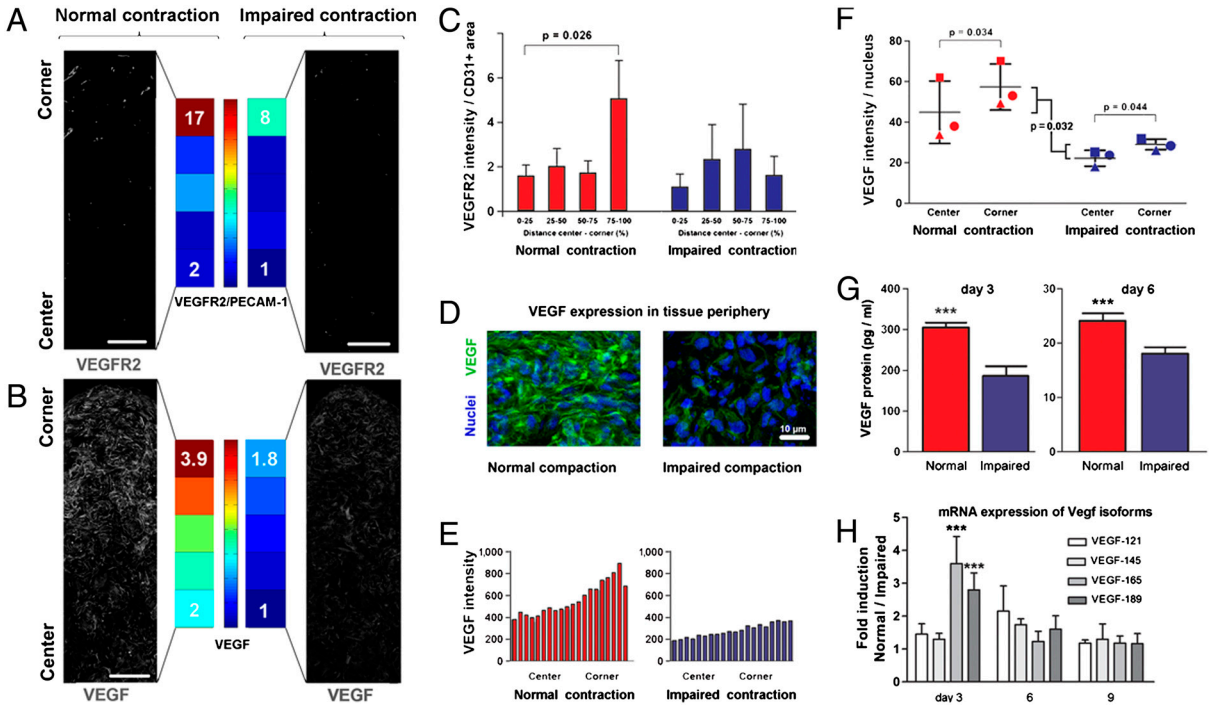

Fig. 4. Tissue contractility spatially regulates the expression of VEGF and VEGFR-2. (*A*, *C*) Upon tissue contraction and deformation, VEGFR-2 is expressed at higher levels in regions of high deformation (*A*, *C*, left, VEGFR-2 fluorescent intensity/PECAM-1$^+$ area, 3.5-fold increase, $n = 15$, $p = 0.026$). This local increase in VEGFR-2 is impaired when tissue contractility is impaired [*A*, *C* right, (scale bars, are 100 μm)]. In regions of high deformation, VEGFR-2 forms clusters at the cellular membrane of EC (Fig. S1). (*B*, *D*, *E*, *F*) Upon normal contraction, a gradient of VEGF forms via local compaction and graded production. (*B*–*E*) Fluorescent intensity is twofold higher in regions of high deformation (*B*–*E*, left; *C* is a close up of corner regions). This observation is confirmed at a mRNA level (Fig. S8*A*). The gradient of VEGF is impaired when tissue contractility is impaired (*B*, *E*, right). (*F*) Upon normalization to the number of nuclei, the fluorescent intensity of VEGF/nucleus is higher in regions of high deformation ($p = 0.034$) and higher in contracting tissues than in tissues whose contraction is impaired ($p = 0.032$, see also Fig. S8*B*). (*G*) The production of VEGF (ELISA assay) is higher in cell pellets undergoing normal contraction than when contraction is impaired ($p < 0.001$). (*H*) Impaired contraction specifically affects the expression of VEGF isoforms 165 and 189 (ECM-binding isoforms). Expression levels of isoforms 121 and 145 (non-ECM-binding isoforms) remain unchanged ($p < 0.001$).

that tissue contraction regulates the expression of VEGF. We concluded that tissue deformation regulates the formation of a VEGF gradient formed via a local tissue compaction and a local regulation of VEGF expression.

Cell-Generated Forces Modulate the Production of ECM Binding Isoforms VEGF$_{189}$ and VEGF$_{189}$. The production of VEGF is regulated via mRNA splicing which induces the formation of various isoforms (26). VEGF isoforms differ in heparin-binding domains (HBD) which affects their capacity to bind to cellular membranes and ECM. Such property could modulate their localization in the extracellular space (26) and is suited for the creation of molecular gradients (27). VEGF$_{121}$, the shortest isoform, lacks HBD, is weakly acidic and freely diffusible upon secretion. VEGF$_{189}$, a longer isoform, has two HBD and is mostly sequestrated in the ECM and at the cell surface. VEGF$_{165}$ possesses intermediate properties, has a moderate affinity for heparin and is both soluble and bounded (26). Using isoform-specific polymerase chain reaction, we observed in cell pellets that VEGF$_{165}$ and VEGF$_{189}$ expression was 2.5-fold higher upon normal contraction as compared to impaired contraction (Fig. 4*H*, $p < 0.001$, $n = 3$). On the opposite, the expression of VEGF$_{121}$ and VEGF$_{145}$ remained unchanged. This observation suggests that tissue deformation influences the expression of longer, heparin-binding VEGF isoforms. We speculate that the ECM and cellular-binding properties of the two isoforms reinforce the formation of the VEGF gradient by preventing protein diffusion.

Tissue Contractility Induces Local Proliferation of Endothelial Cells. Because tissue deformation regulates the microenvironmental concentration of VEGF-A and VEGFR-2 and because VEGF-A is a potent mitogen acting via VEGFR-2, we quantified the local proliferation of EC. Using pulsed exposure to EdU (5-ethynyl-2'-deoxyuridine) (5-ethynyl-2'-deoxyuridine exposure over twelve hours, daily time point over five days), we observed that EdU$^+$ cells were limited to PECAM-1$^+$ cells. EdU$^+$ cells represented 0.3 to 1% of the total cell number (Fig. S10). Upon tissue defor-

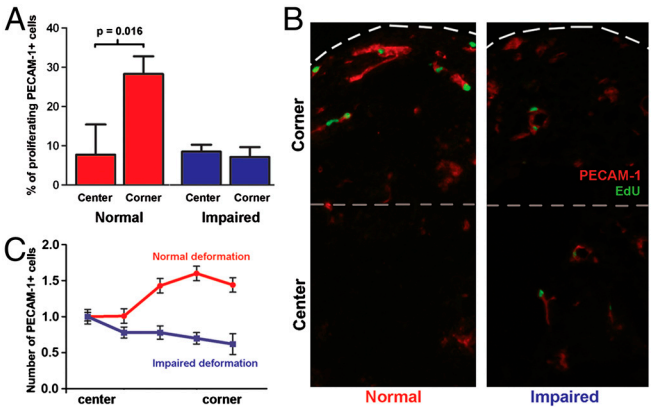

Fig. 5. Tissue deformation induces a local differential on endothelial cell proliferation. (*A*, *B*) EdU pulsed incorporation shows a higher percentage of proliferating EC in regions of high deformations. This local differential in EC proliferation is abolished when tissue deformation is impaired. (*C*) VS in regions of high deformation include a higher number of EC in deforming tissues as compared to tissues whose deformation is impaired.

mation, VS in regions of high deformation included more proliferating cells (EdU^+) than VS in the tissue center (Fig. 5 *A* and *B*, 28% vs. 8%, $p = 0.016$). When deformation was impaired, the density of proliferating cells was lower (8%) and their distribution homogenous (Fig. 5 *A* and *B*). Finally, we quantified the number of PECAM-1^+ cells per VS. Upon normal deformation, the number of PECAM-1^+ cells in VS increased from tissue center to corner (Fig. 5*C*). When contraction was impaired, the number of PECAM-1^+ cells in VS remained unchanged (Fig. 5*C*). VS in tissue corners included more PECAM-1^+ cells upon normal contraction as compared to impaired contraction (Fig. 5*C*). We concluded that VS in regions of high deformation formed via a higher EC proliferation which resulted in a higher number of cells per VS.

We propose that tissue deformation can spatially modulate the expression of VEGF-A and VEGFR-2, and contribute to the formation of patterns of VS by inducing local differentials in EC proliferation.

Discussion

Vascular patterns can emerge from the spatial regulation of angiogenic signals including the concentration of and the EC sensitivity to mitogens (5, 28). Here, we suggest that tissue contraction and deformation can spatially modulate cellular density, the local expression of VEGF-A and VEGFR-2, and induce a local differential in EC proliferation.

Morphogen gradients form by regulated production, retention, controlled release, diffusion, and degradation (12, 29). Our data suggest that interstitial cells can form gradients of angiogenic microenvironments via local tissue compaction and a local regulation of VEGF signaling. The regulation of ECM-binding VEGF isoforms ($VEGF_{165}$ and $VEGF_{189}$) by tissue contractility could prevent VEGF protein diffusion and reinforce molecular gradients (30).

The agonist activity of VEGF on VEGFR-2 (*i*) guides the sprouting of the cell situated at the tip of the VS via local gradients (filopodia/lamellipodia extension along a differential of concentration) and (*ii*) induces the proliferation of the following, stalk EC based on local concentration (absolute concentration) (12). Our observations suggest that the higher local concentration of VEGF and of the local expression of the corresponding receptor VEGFR-2 induced a local differential in the proliferation of the stalk cells. Previous studies revealed that EC shape and cytoskeletal tension regulates a discrete cell cycle check-point at the G1/S border. The sensitivity to a mitogen is partly modulated by mechanical factors via the cdk inhibitor p27 and the activator cyclin D (31, 32). We speculate that the local proliferation of EC results from an appropriate combination of cytoskeletal tension and VEGF-A/VEGFR-2 density.

This experiment links tissue contraction and deformation to the formation of a gradient of angiogenic microenvironments. This correlation might explain, in further investigations, how contractile forces generated within a tissue or between adjacent tissues might have a long-range control over capillary formation. These findings may be relevant in wound healing -vascular morphogenesis was reported to be mechanically driven by the contracting wound (2)-, or in cancer biology -tumors are dependent on angiogenesis and stiffer than normal tissues due to an elevated endogeneous tension (33).

Self-organization can emerge from tissue contractility and geometry. Such properties induce an heterogeneous tissue deformation and pattern the behavior of cells. We suggest that tissue contractility and deformation can modulate the formation of gradients of angiogenic microenvironments and angiogenesis. We speculate that such a mechanism might contribute to the long-range patterning of the vascular system.

Methods

Agarose Chips. Micropatterned agarose chips for nonadherent cell culture were formed by replica molding. Patterned elastomeric stamps of poly (dimethylsiloxane) (PDMS; Sylgard 184, Dow Corning) were replicated from either etched silicon wafers or SU-8/silicon wafers. PDMS stamps were used to routinely replicate the microstructures in 4% agarose.

Coculture. A coculture of 92% hMSC and 8% huvEC was used for all experiments. The culture medium for the coculture (Exp. Medium) was serum-free and composed of Dulbecco's Modified Eagle's Medium supplemented with 10^-7 M dexamethasone, 50 mg/mL ascorbate 2-phosphate, 40 mg/mL proline, 100 mg/mL pyruvate, and 50 mg/mL ITS 1 Premix (Becton-Dickinson, MA: 6.25 mg/mL insulin, 6.25 mg/mL transferrin, 6.25 ng/mL selenious acid, 1.25 mg/mL bovine serum albumin, 5.35 mg/mL linoleic acid).

ACKNOWLEDGMENTS. We thank M. Berger, K. Ma for their technical suggestions and assistance; H.Tank and J. de Boer for comments on the manuscript. This work was supported by funds from the STW (Stichting Technologie en Wetenschappen), The Netherlands, project TKG 6716.

1. Perryn ED, Czirok A, Little CD (2008) Vascular sprout formation entails tissue deformations and VE-cadherin-dependent cell-autonomous motility. *Dev Biol* 313:545–555.
2. Kilarski WW, Samolov B, Petersson L, Kvanta A, Gerwins P (2009) Biomechanical regulation of blood vessel growth during tissue vascularization. *Nat Med* 15:657–664.
3. Tzima E, et al. (2005) A mechanosensory complex that mediates the endothelial cell response to fluid shear stress. *Nature* 437:426–431.
4. Nelson CM, Chen CS (2003) VE-cadherin simultaneously stimulates and inhibits cell proliferation by altering cytoskeletal structure and tension. *J Cell Sci* 116:3571–3581.
5. Mammoto A, et al. (2009) A mechanosensitive transcriptional mechanism that controls angiogenesis. *Nature* 457:1103–1108.
6. Ingber DE (2002) Mechanical signaling and the cellular response to extracellular matrix in angiogenesis and cardiovascular physiology. *Circ Res* 91:877–887.
7. Herbert SP, Stainier DY (2011) Molecular control of endothelial cell behavior during blood vessel morphogenesis. *Nat Rev Mol Cell Biol* 12:551–564.
8. Chen CS, Mrksich M, Huang S, Whitesides GM, Ingber DE (1997) Geometric control of cell life and death. *Science* 276:1425–1428.
9. Nelson CM, et al. (2005) Emergent patterns of growth controlled by multicellular form and mechanics. *Proc Natl Acad Sci USA* 102:11594–11599.
10. Shay-Salit A, et al. (2002) VEGF receptor 2 and the adherens junction as a mechanical transducer in vascular endothelial cells. *Proc Natl Acad Sci USA* 99:9462–9467.
11. Shweiki D, Itin A, Soffer D, Keshet E (1992) Vascular endothelial growth factor induced by hypoxia may mediate hypoxia-initiated angiogenesis. *Nature* 359:843–845.
12. Gerhardt H, et al. (2003) VEGF guides angiogenic sprouting utilizing endothelial tip cell filopodia. *J Cell Biol* 161:1163–1177.
13. Rivron NC, et al. (2009) Tissue assembly and organization: developmental mechanisms in microfabricated tissues. *Biomaterials* 30:4851–4858.
14. Laib AM, et al. (2009) Spheroid-based human endothelial cell microvessel formation in vivo. *Nat Protoc* 4:1202–1215.
15. Engler AJ, Sen S, Sweeney HL, Discher DE (2006) Matrix elasticity directs stem cell lineage specification. *Cell* 126:677–689.
16. Zisa D, Shabbir A, Suzuki G, Lee T (2009) Vascular endothelial growth factor (VEGF) as a key therapeutic trophic factor in bone marrow mesenchymal stem cell-mediated cardiac repair. *Biochem Biophys Res Commun* 390:834–838.
17. Furumatsu T, et al. (2003) Vascular endothelial growth factor principally acts as the main angiogenic factor in the early stage of human osteoblastogenesis. *J Biochem* 133:633–639.
18. Rouwkema J, de Boer J, Van Blitterswijk CA (2006) Endothelial cells assemble into a 3-dimensional prevascular network in a bone tissue engineering construct. *Tissue Eng* 12:2685–2693.
19. Knapp DM, Barocas VH (2004) Estimation of cell traction and migration in an isometric cell traction assay. *AIChE J* 45:2628–2640.
20. Sieminski AL, Hebbel RP, Gooch KJ (2004) The relative magnitudes of endothelial force generation and matrix stiffness modulate capillary morphogenesis in vitro. *Exp Cell Res* 297:574–584.
21. Lecuit T, Lenne PF (2007) Cell surface mechanics and the control of cell shape, tissue patterns and morphogenesis. *Nat Rev Mol Cell Biol* 8:633–644.
22. Rivron NC, Liu JJ, Rouwkema J, de Boer J, van Blitterswijk CA (2008) Engineering vascularised tissues in vitro. *Eur Cell Mater* 15:27–40.
23. McBeath R, Pirone DM, Nelson CM, Bhadriraju K, Chen CS (2004) Cell shape, cytoskeletal tension, and RhoA regulate stem cell lineage commitment. *Dev Cell* 6:483–495.
24. Yung YC, Chae J, Buehler MJ, Hunter CP, Mooney DJ (2009) Cyclic tensile strain triggers a sequence of autocrine and paracrine signaling to regulate angiogenic sprouting in human vascular cells. *Proc Natl Acad Sci USA* 106:15279–15284.
25. Beerepoot LV, Shima DT, Kuroki M, Yeo KT, Voest EE (1996) Up-regulation of vascular endothelial growth factor production by iron chelators. *Cancer Res* 56:3747–3751.
26. Giacca M (2010) Non-redundant functions of the protein isoforms arising from alternative splicing of the VEGF-A pre-mRNA. *Transcr* 1:149–153.
27. Ferrara N (2010) Binding to the extracellular matrix and proteolytic processing: two key mechanisms regulating vascular endothelial growth factor action. *Mol Biol Cell* 21:687–690.

28. Ozawa CR, et al. (2004) Microenvironmental VEGF concentration, not total dose, determines a threshold between normal and aberrant angiogenesis. *J Clin Invest* 113:516–527.
29. Wolpert L (1969) Positional information and the spatial pattern of cellular differentiation. *J Theor Biol* 25:1–47.
30. Carmeliet P (2003) Angiogenesis in health and disease. *Nat Med* 9:653–660.
31. Huang S, Chen CS, Ingber DE (1998) Control of cyclin D1, p27(Kip1), and cell cycle progression in human capillary endothelial cells by cell shape and cytoskeletal tension. *Mol Biol Cell* 9:3179–3193.
32. Huang S, Ingber DE (2002) A discrete cell cycle checkpoint in late G(1) that is cytoskeleton-dependent and MAP kinase (Erk)-independent. *Exp Cell Res* 275:255–264.
33. Paszek MJ, et al. (2005) Tensional homeostasis and the malignant phenotype. *Cancer Cell* 8:241–254.

Supporting Information

Rivron et al. 10.1073/pnas.1201626109

SI Methods

Cell Culture and Reagents. ***Human mesenchymal stem cells.*** Human Bone marrow aspirates are obtained from donors after written informed consent, and human Mesenchymal Stem Cells (hMSCs) are isolated as follows. Aspirates are resuspended by using 20-gauge needles, plated at a density of 5×10^5 cells per square centimeter and are cultured in hMSC proliferation medium containing α-MEM (Life Technologies), 10% FBS (Cambrex), 0.2 mM ascorbic acid (Asap; Life Technologies), 2 mM l-glutamine (Life Technologies), 100 units/mL penicillin (Life Technologies), 10 μg/mL streptomycin (Life Technologies), and 1 ng/mL basic FGF (Instruchemie). Cells are grown at 37 °C in a humid atmosphere with 5% CO_2. Medium is refreshed twice a week, and cells are used for further subculturing or cryopreservation. For experiments, the hMSC medium (termed Exp. Medium) is serum-free and composed of Dulbecco's Modified Eagle's Medium supplemented with $10^{-}7$ M dexamethasone, 50 mg/mL ascorbate 2-phosphate, 40 mg/mL proline, 100 mg/mL pyruvate, and 50 mg/mL ITS1+Premix (Becton-Dickinson, MA: 6.25 mg/mL insulin, 6.25 mg/mL transferrin, 6.25 ng/mL selenious acid, 1.25 mg/ml bovine serum albumin, 5.35 mg/mL linoleic acid).

Human umbilical vein endothelial cells. Human umbilical vein endothelial cells (HUVECs) are purchased from Lonza (Lonza, group Ltd. Switzerland). Cells are grown at 37 °C in a humid atmosphere with 5% carbon dioxide (CO2) in endothelial growth medium-2 (Cambrex). Cells are routinely split at a 1:5 ratio and cultured in fewer than five passages. Only HUVECs from passage 3 or 4 are used to seed the coculture experiments.

MicroWell Array (MWA) and Shaped Well Array (SWA) Agarose chips. Micropatterned agarose chips for nonadherent cell culture are formed by replica molding. MWA: silicon wafers are etched to form cylindrical wells of 200 um diameter and 160 um deep. The interspace between wells is 100 um. Each chip contains 2,865 wells and a total diameter of 11.5 mm. SWA: SU-8 photoresist is patterned on top of a silicon wafer by depositing three layers to obtain a total height of 700 um. Wells are geometric (circle, square, triangle) and have a constant surface area of 1 mm^2. One SWA includes 15 geometric wells and has a total diameter of 11.5 mm. Structures from MWA and SWA are replicated in poly(dimethylsiloxane) (PDMS; Sylgard 184, Dow Corning) with a total thickness of 8 mm, individual chips are punched, cleaned, and sterilized in ethanol. Routinely, in the laminar flow cabinet, the PDMS stamps are deposited in the center of the well of a 6-well plate (microstructures on top) and a boiling solution of 3% agarose (Ultra pure agarose, Invitrogen) is poured on the PDMS stamp (8 mL), quickly centrifugated ($1,300 \times g$ for 1 min) to remove air bubbles and let to solidify. Upon solidification, agarose chips are demolded using a spatula and sterile gloves, punched to 11.5 mm diameter and placed in a 12 well plate. After wetting using corresponding Exp. medium (500 microliters), a concentrated suspension of cells (0.4 millions) is seeded, allowed to settle for 15 min on the chip and 1.5 milliliters of Exp. medium is then added. Cell clusters (approximately 500 cells/cell cluster) spontaneously fuse within 24 h are cultured for 150 h. Half of the medium is changed every day of culture. After 150 h, cell clusters are flushed out using Exp. medium, centrifuged ($340 \times g$, 1 min), resuspended in the Exp. medium and seeded on the SWAs. 20,000 cell clusters are seeded per SWA. Clusters are allowed to settle in the wells for 1 min then centrifuged ($340 \times g$, 1 min). Cell clusters which do not settle in the wells are harvested using a pipet and seeded again. For optimal seeding, 2–3 rounds of seeding are done. 1.5 mL of Exp. medium is added. Half of the medium is changed every day of culture. Cell clusters fuse within 24 h. Resulting tissues contain approximately 200.000 cells, have a surface area of 1 mm^2, and a thickness of 250 um.

Coculture. A coculture of 92% hMSC and 8% huvEC in Exp. Medium (as described above) are used for all experiments. Half the medium is replaced every day. Blebistatin (50 mM, Sigma-Aldricht) and Y-27632 (10 mM, Calbiochem) are added 24 h after seeding microscale clusters on the SWA. Half the medium is replaced every day with constant total concentrations of 50 mM of Blebistatin and 10 uM of Y-27632 until day 5. VEGF scavenging is supplemented to the culture medium at 2 μg/mL. The anti-rh-VEGF (R&D systems) antibody which binds both to VEGF165 and VEGF121. Pellet culture for the experiments of Fig. 4 *G* and *H* are done by pulling 0.5 million cells (92% hMSC and 8% huvEC) in a 10 mL tube, centrifuging to form a pellet ($340 \times g$, 2 min). 5 mL of medium is added. Pellets rounded up and form a sphere within 48 h and are cultured for 6 d.

Immunohistochemical Analysis. Tissue are cultured for 5 d after seeding on the SWA with or without Y27632+Blebistatin. After harvesting, tissues are frozen in Cryomatrix at −60 °C. Sections (7 μm) are cut with a cryotome. Sections are fixed in cold acetone for 5 min and air-dried. Sections are rehydrated for 10 min, after which they are incubated for 30 min with 10% FBS in PBS to block nonspecific background staining. Sections are incubated with monoclonal mouse antihuman PECAM-1 antibody (Dako), a monoclonal rabbit antihuman VEGF Carboxyterminal end antibody (Abcam), a monoclonal rabbit antihuman VEGFR2 antibody (Cell Signaling), a rabbit antihuman HIF1a antibody (Abcam), Phalloidin-Alexa fluor 488 conjugated antibody (Invitrogen), or a monoclonal mouse antihuman Phospho-Myosin Light Chain 2 (Ser19) (Cell signaling technology) for 1 to 4 h. Sections are washed in PBS and subsequently incubated with the secondary antibody (Alexa Fluor 488 or 594 antibody, Invitrogen). Samples are counterstained with Dapi (Sigma). Cellular proliferation is assessed by EdU (5-ethynyl-2'-deoxyuridine) incorporation over a period of 12 h ending at 24, 96, and 144 h of culture. The cell proliferation assay is performed using the Click-iT™ EdU kit (Invitrogen). Pictures are taken using a confocal microscope (Leica LSM500). To prevent biased measurements, quantifications of the area of PECAM-1^+ cells on Figs. 3 and 4 are done using a threshold applied on images based on size and circularity (Image J) to select for the PECAM-1^+ structures which elongated in the main plane of the tissue. Thresholded PECAM-1^+ structures are termed vascular structures (VS). Quantification on Fig. S5 is done without a threshold. For quantification of Figs. 3 and 4, each image is divided into 20 boxes from the center to the periphery. Each box is used for quantification of either the number of nuclei, the area of VS, the intensity of VEGF fluorescence, or the intensity of the VEGFR-2 fluorescence. Results are the average of five nonconsecutive cuts for each three different biological samples. Results are used to create the 20 boxes-graphics presented in Fig. 3*B* or pooled to create graphics (Fig. 3 *A*, *D*; Fig. 4 *A*–*F*). Color maps (Fig. 3) show values, in five consecutive regions ranging from the tissue center to the tissue corners, of VS density (scale from 1 to 4.8) and VS/nucleus density (scale from 1 to 2.5) normalized to the central region. The same scale is used for normal and impaired compaction. Contribution of tissue density to VS density is measured as

the expected VS density due to a strict effect of compaction as compared to experimental VS density. Color maps (Fig. 4) show values for VEGF density per nucleus (scale 1 to 3) and VEGFR2 intensity per PECAM-1$^+$ area (scale 1 to 17) in five consecutive regions ranging from the tissue center to the tissue corner and normalized to the region of weakest intensity (central region, impaired compaction).

ELISA Assay. ELISA assay (R&D systems) was performed as described by the manufacturer.

Gene Expression Analysis by qPCR. The effect of tissue contraction and deformation on expression of angiogenic marker genes was analyzed from tissues cultured for 3 d on the SWA. RNA was isolated from a pool of five tissues by snap freezing the tissues in liquid nitrogen, crunching them using a pestle and by using an RNeasy mini kit (Qiagen). qPCR was performed by using SYBR green (Invitrogen) on a Light Cycler (Roche). Data were analyzed by using Light Cycler software version 3.5.3, using the fit point method by setting the noise band to the exponential phase of the reaction to exclude background fluorescence. Expression of angiogenic marker genes was calculated relative to DAPDH rRNA levels by the comparative ΔCT method. Primers were obtained from SAS Bioscience and used according to the manufacturer's protocol. Primers for VEGF isoforms had the following sequences:

human VEGF165 sense: ATCTTCAAGCCATCCTGTGTGC
human VEGF165 antisense: CAAGGCCCACAGGGATTTTC
human VEGF189 sense: ATCTTCAAGCCATCCTGTGTGC
human VEGF189 antisense: CACAGGGAACGCTCCAGGAC
human VEGF121 sense: GCGGATCAAACCTCACCAAG
human VEGF121 antisense: TCGGCTTGTCACATTTTTCTTG
human VEGF145 sense: GAATGCAGACCAAAGAAAGATAGAG
human VEGF145 antisense: TCGGCTTGTCACATACGCTCC

Statistics. Differences between groups are determined using a Student's T-test as described for each figure.

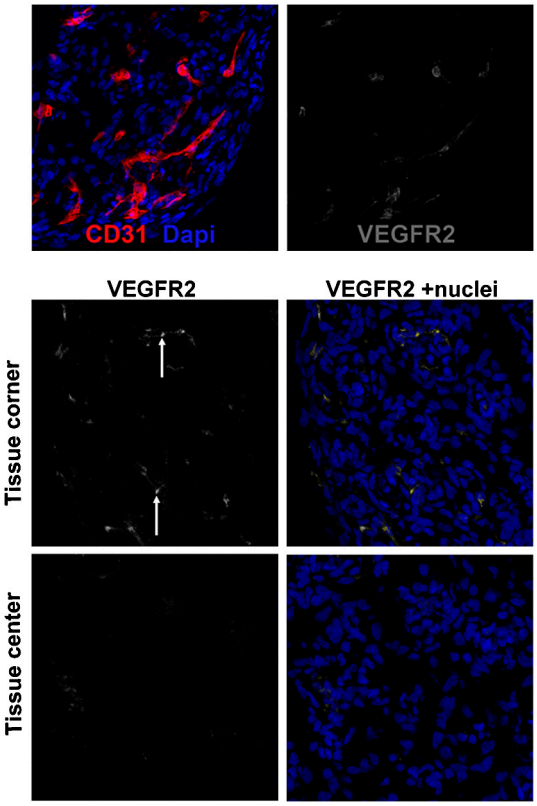

Fig. S1. VEGFR2+ cells strictly overlaps with PECAM-1$^+$ cells and form clusters in regions of high deformation. Top row: double staining for PECAM-1 and VEGFR2 shows that VEGFR2 expression is restricted to the PECAM-1$^+$ cells. Middle and bottom rows: VEGFR2 staining shows the formation of clusters of VEGFR2 at the cellular membrane, in regions of high deformation (middle row). Such clusters are not observed in the central region of the tissue (bottom row).

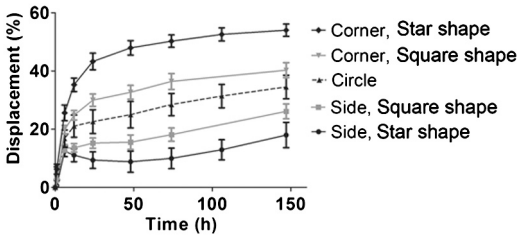

Fig. S2. Tissue displacement. The displacement of tissue borders is measured as relative to the initial distance between the center and the border using bright field pictures ($n = 5$). Displacement = 100% of the original distance. Standard deviations, $n = 10$.

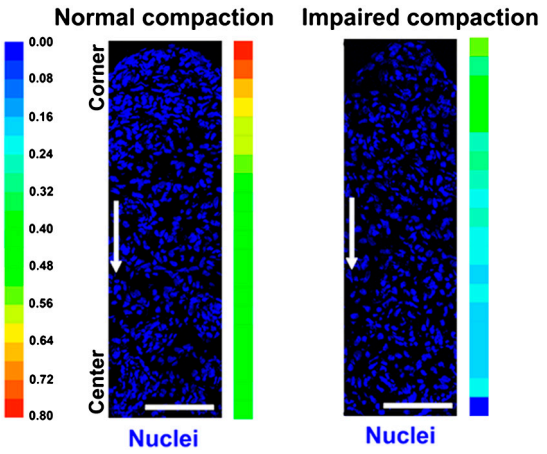

Fig. S3. Theoretical estimation of local strains. Local strains are estimated in star-shaped tissues for a strip from the center of the tissue to the corner (as displayed in Figs. 3, 4), based on nuclear density and macroscopic overall strain. As determined by light microscopy, normally contracting tissues display an overall strain of 0.54, whereas the overall strain is reduced to 0.27 in tissues with an impaired contraction. Based on these numbers, the average nuclear density in the unstrained state is estimated by dividing the average nuclear density in the strained state by 1 minus the overall strain. Finally, the local strains in twenty slices is determined by relating the local nuclear density in the strained state with the average nuclear density in the unstrained state.

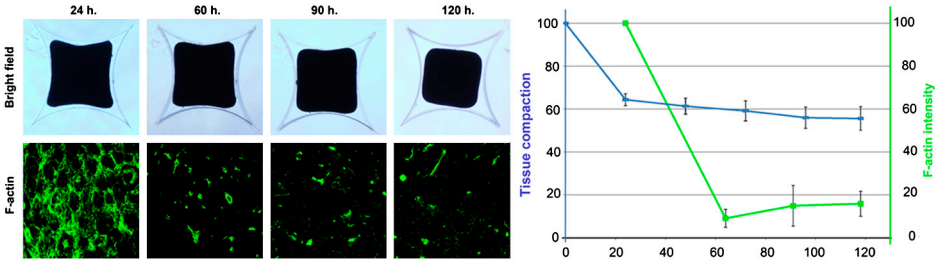

Fig. S4. The timeline of tissue compaction correlates with the F-actin intensity. Tissue contraction is assessed using bright field images and is quantified by measuring the projected area of tissues overtime ($n = 5$). F-actin fluorescent intensity is assessed using a phalloidin staining and is quantified using an histogram plot (Image J) (Standard deviations, $n = 5$).

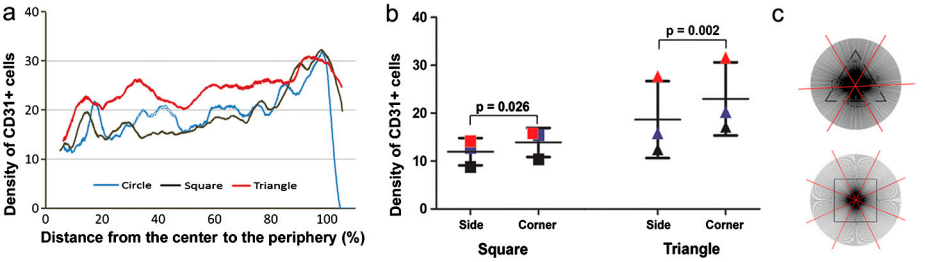

Fig. S5. Density of PECAM-1$^+$ cells. Radial-Profile Plot are done using five images of the total cross-section of a tissue for three different biological samples. Image J (http://rsbweb.nih.gov/ij/) is used to produce a profile plot of normalized integrated intensities around concentric circles as a function of distance from a point in the image. The intensity at any given distance from the point represents the sum of the pixel values around a circle. This circle has the point as its center and the distance from the point as radius. The integrated intensity is divided by the number of pixels in the circle that is also part of the image, yielding normalized comparable values (see details in http://rsb.info.nih.gov/ij/plugins/radial-profile.html). Shapes are divided into six or eight equal areas, as depicted by the red spokes (right schematics), values from each spoke and each area are averaged. The value is the average for one samples side and its respective corners. The statistical significance is calculated using a T-Test (one tail distribution, paired, standard deviations, $n = 3$).

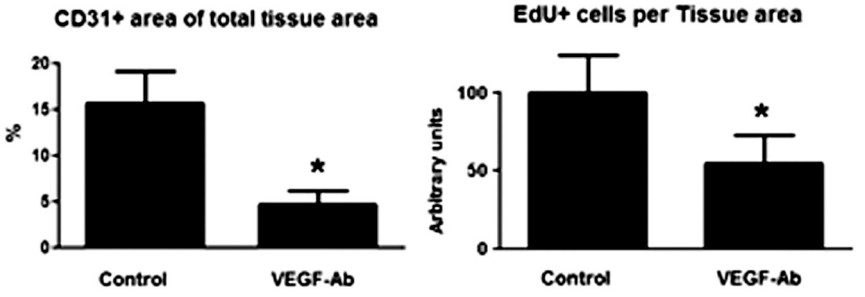

Fig. S6. VEGF scavenging with an antibody decreases PECAM1+ area and proliferation. In cell pellets, we observed that the scavenging of endogeneous VEGF using an antibody induces a decrease in the area covered by PECAM1+ cells and a decrease in cellular proliferation (EdU incorporation). Student T-Test, $n = 2$.

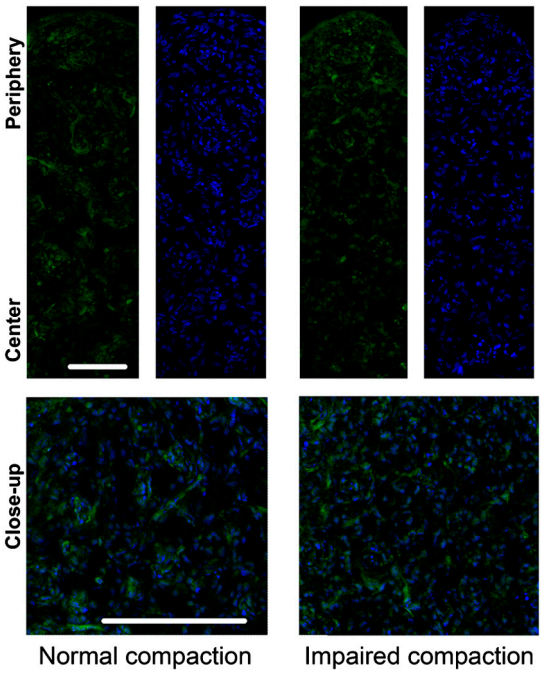

Fig. S7. Tissue hypoxia is homogeneous. Vascular morphogenesis is driven by local hypoxia which attract blood vessels through the activation of HIF1a which regulates VEGF production. HIF1a is constantly produced and degraded in the cytoplasma of cells and translocate to the nucleus upon hypoxia. Here, using antibody staining, we found that HIF1a is partly cytoplasmic and homogeneously expressed across the tissues. The homogenous expression of HIF1a suggests that the gradient of VEGF is not controlled by an underlying gradient of hypoxia. Scale bars are 100 micrometers.

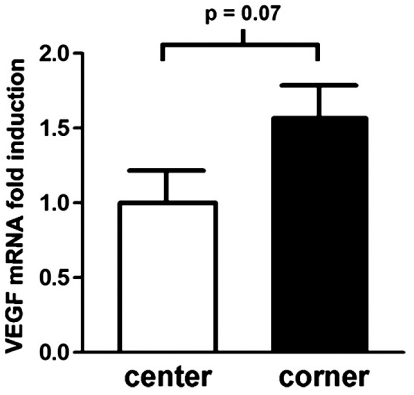

Fig. S8. VEGF expression. The corners of microfabricated tissues are dissected under a microscope and are separated from the center of the tissues (day 5 on SWA, $n = 15$ microfabricated tissues). qRT-PCR for VEGF-A mRNA is performed ($n = 3$ groups) as described in *Methods* (main text). VEGF-A mRNA is 1.5 times higher in tissue corners as compared to tissue centers (n.s. $p = 0.07$).

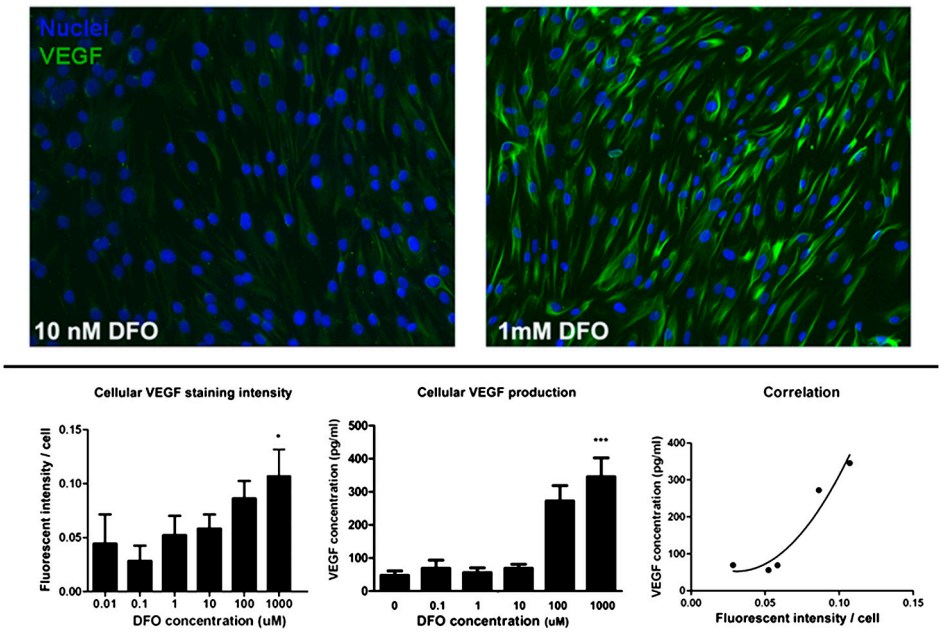

Fig. S9. A twofold increase in VEGF immunofluorescent intensity correlates with a fivefold increase in VEGF protein concentration. We tested the correlation between VEGF immunofluorescent intensity and VEGF protein concentration. Deferoxamine (DFO, a HIF-1a inducer) lead to a twofold increase in VEGF immunofluorescent staining intensity (top row and bottom left). In these samples, we assessed the production of VEGF protein by ELISA assay on cell lysates (ELISA assay for isoforms 165 and 121). This twofold increase in fluorescent intensity correlated with a fivefold increase in the intracellular production of VEGF (bottom middle). The correlation between fluorescent intensity and VEGF protein concentration was linear in the ranged depicted in this study (bottom right).

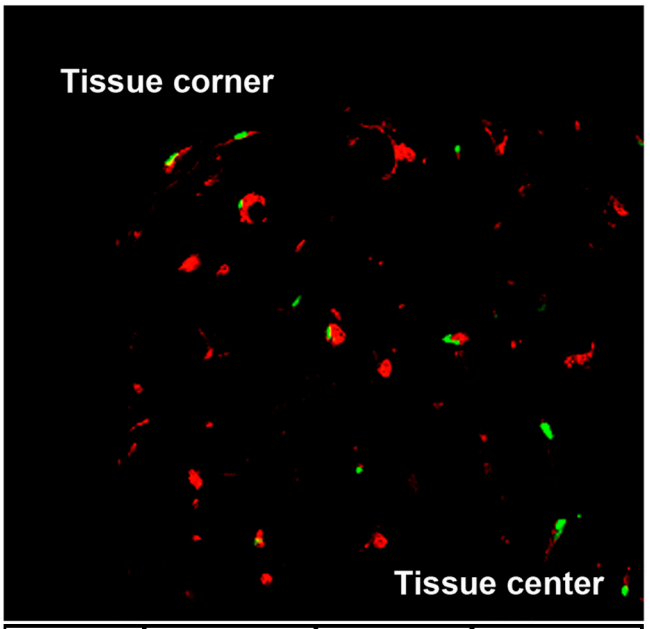

	24 hours	96 hours	144 hours
Circle	0.34 +/- 0.22	1.03 +/- 0.42	0.42 +/- 0.26
Triangle	0.49 +/- 0.14	0.38 +/- 0.24	0.63 +/- 0.15

Fig. S10. Cellular proliferation. Cellular proliferation was assessed by EdU incorporation over a period of 12 h ending at 24, 96, and 144 h of culture and measured as a percentage of the total number of cells. Proliferating cells (green) are restricted to the PECAM-1$^+$ cells and are not limited to the tissue periphery (Standard deviations, $n = 3$).